Atmos. Meas. Tech. Discuss., 7, 11439–11479, 2014
www.atmos-meas-tech-discuss.net/7/11439/2014/
doi:10.5194/amtd-7-11439-2014

Atmospheric Measurement Techniques Discussions

A one year comparison of 482 MHz radar wind profiler, RS92-SGP Radiosonde and 1.5 µm Doppler Lidar wind measurements

E. Päschke, R. Leinweber, and V. Lehmann

DWD, Meteorologisches Observatorium Lindenberg – Richard Aßmann Observatorium, Lindenberg, Germany

Received: 14 October 2014 – Accepted: 20 October 2014 – Published: 19 November 2014

Correspondence to: E. Päschke (eileen.paeschke@dwd.de)

Published by Copernicus Publications on behalf of the European Geosciences Union.

Abstract

We present the results of a one-year quasi-operational testing of the 1.5 µm StreamLine Doppler lidar developed by Halo Photonics from 2 October 2012 to 2 October 2013. The system was configured to continuously perform a velocity-azimuth display (VAD) scan pattern using 24 azimuthal directions with a constant beam elevation angle of 75°. Radial wind estimates were selected using a rather conservative signal-to-noise ratio (SNR) based threshold of −18.2 dB (0.015). A 30 min average wind vector was calculated based on the assumption of a horizontally homogeneous wind field through a singular-value decomposed Moore–Penrose pseudoinverse of the overdetermined linear system. A strategy for a quality control of the retrieved wind vector components is outlined which is used to ensure consistency between the retrieved winds and the assumptions inherent to the employed wind vector retrieval. Finally, the lidar measurements are compared with operational data from a collocated 482 MHz radar wind profiler running in a four-beam Doppler beam swinging (DBS) mode and winds from operational radiosonde measurements. The intercomparisons show that the Doppler lidar is a reliable system for operational wind measurements in the atmospheric boundary layer (ABL).

1 Introduction

The wind field is one of the most important atmospheric parameters. Its accurate measurement with a high spatial and temporal resolution is crucial for operational Numerical Weather Prediction (NWP) models and it is of course also vital for numerous other applications. The operational remote sensing of the vertical wind profile is currently dominated by radar wind profilers (RWP), with frequencies ranging from L-band to VHF. Here, the letter codes L and VHF (Very High Frequency) are standard band designations according to the IEEE standard radar-frequency letter-band nomenclature.

AMTD
7, 11439–11479, 2014

Recently, a new generation of portable infrared (IR) Doppler lidar (DL) systems based on fiber-optic technology developed for the telecommunications industry has become commercially available. In contrast to conventional DL designs based on free-space optics, the use of fiber-optic elements considerably simplifies fabrication, alignment and long-term stability. While there is currently a large market demand for such systems from the renewable energy sector, it is also interesting to test the capabilities of these new instruments for possible future operational boundary layer wind profiling, complementary to radar profilers.

Previous intercomparisons of DL and RWP winds have generally shown good agreements (Cohn and Goodrich, 2002; Pearson et al., 2009; Shaw et al., 2003). These intercomparisons, however, were always based on temporally short-term measurement periods. For example, Cohn and Goodrich (2002) have shown from a measurement period of 2.3 h that the differences of the Doppler velocities obtained with a 915 MHz boundary layer RWP and the NOAA High Resolution Doppler Lidar (HRDL) had a standard deviation of about $\sigma_r = 0.20$–$0.23\,\mathrm{m\,s^{-1}}$, which was attributed to turbulent variability and instrumental noise. A translation of this error into the corresponding error for the horizontal wind resulted in an error of less than 0.11–$0.27\,\mathrm{m\,s^{-1}}$ for a 30 min measurement period, depending on the beam pointing sequence (five-beam or three-beam pointing DBS configuration). Pearson et al. (2009) compared wind measurements from a 9 min Doppler lidar scan and radar data from a 10 min average for four different times which also showed very good level of agreement, except for somewhat less well correlated wind speed data, which was attributed to insects or ground clutter contamination of the radar velocity data. A month long field study has been carried out in the Salt Lake Valley (Shaw et al., 2003). Here wind measurements have been collected with a 915 MHz RWP and a pulsed DL ($\lambda = 10.59\,\mu\mathrm{m}$). Comparisons of half-hour consensus winds obtained with the RWP with corresponding VAD winds from DL showed broad agreement albeit considerable scatter, which was attributed to the different sampling volumes of the two systems.

AMTD
7, 11439–11479, 2014

The article describes the setup and methodology of the test, with a focus on aspects of data processing based on the systems direct output and the results of the comparison statistics derived from about 17 000 wind profiles that have been obtained over the course of a year. To the author's knowledge such long time comparisons between Doppler lidar and radar wind profiler have not been done so far and thus may give valuable and more representative insights into the performance of Doppler lidar wind measurements. The paper is structured as follows: in Sect. 2 information describing the data set used for the analysis are given. It includes detailed information related to instrumentation and, above all, the data processing and quality control. In Sect. 3 the statistics of one year long DL measurements are discussed in comparison to RWP and radiosonde (RS) measurements. An interesting type of "gross error" due to a range ambiguity effect is dicussed in Sect. 4. Finally, Sect. 5 presents a summary of the results and conclusions.

2 Data set

The intercomparison period used for our analysis is from 2 October 2012 to 2 October 2013. The wind data were collected at the Lindenberg Meteorological Observatory – Richard Aßmann Observatory (RAO). At this site RWP and radiosonde winds are routinely measured and provided for assimilation into a number of NWP models. Since September 2012, a 1.5 µm DL is being tested with regard to the efficient allocation of this measurement system for operational wind profiling within the atmospheric boundary layer (ABL). With a spatial separation of about 30 m the installation of the DL was as close as possible to the RWP. These circumstances create outstanding conditions for the instruments intercomparison. Further informations on the single measurement systems are given below.

AMTD
7, 11439–11479, 2014

2.1 Instrumentation overview

In the following a short description of the measuring principles and some technical aspects for each of the instruments used is provided.

2.1.1 1.5 µm Doppler Lidar

The DL emits laser pulses in the near infrared which scatter off particles suspended in the atmosphere, like aerosols and clouds. Data availability is therefore linked to the presence of such particles. The backscattered light has a Doppler shift due to the movement of these particles which can be detected by optical heterodyning in the receiver. Assuming that the target is following the wind, the horizontal wind vector can be determined from the measured line-of-sight (LOS) Doppler wind values. The technical specifications of the StreamLine Doppler lidar developed by Halo Photonics are listed in Table 1. The PRF value implies a maximum unambiguous range of about 10 km. For wind measurements, a VAD scan pattern was set-up as illustrated in Fig. 1. The sketch is limited to $n = 12$ beam pointing directions or rays, however, the measurement scan pattern was using $n = 24$ azimuthal positions with a constant elevation angle $\varepsilon = 75^{\circ}$. Measurements of Doppler velocities $V_r(R, \alpha, t)$ were thus made along a circle at 15° constant intervals of azimuth α. R indicates the range of the measurement, i.e. the distance of the backscattering volume along LOS, and t denotes the time of the measurement. For each of the 24 rays a total of 75 000 laser shots have been emitted. The dwell time for one ray was about 5 s. Taking the time for the scanner to move into account, one full scan lasted about 3 min. For $\varepsilon = 75^{\circ}$, the range gate length of $\Delta R = 48$ m translates to a vertical resolution of about $\Delta Z = 46$ m.

2.1.2 482 MHz radar wind profiler

While the measurement principle of the RWP is also based on the Doppler effect, the significantly longer wavelength of 62 cm makes it possible to obtain measurable echoes

AMTD
7, 11439–11479, 2014

from both the particle-free (clear) atmosphere as well as from the particle-laden atmosphere (clouds and precipitation). The passive phased array antenna of the system is designed to steer the beam into five different directions (vertical and four obliques with an elevation angle of 74.8°). In the operational configuration, the RWP cycles continuously through the four oblique beam directions. The operational set-up uses two different pulse widths to obtain data with different radial resolutions (low and high mode). Eventually, a total of five cycles per mode is used to generate 30 min averaged profiles. The averaging algorithm used is called "consensus averaging" (Fischler and Bolles, 1981; Strauch et al., 1984) and is applied to each beam direction separately. This algorithm facilitates discrimination between "good" and "bad" estimates in the low SNR regime (Frehlich and Yadlowsky, 1994). For the purpose of this study, only data from the low mode with a pulse width of $\tau = 1000$ ns are considered. RWP low mode measurements are available for a total of 96 range gates extending from 450 m up to 9380 m. The radial and the vertical resolution of one range gate is $\Delta R = 150$ m and $\Delta Z = 145$ m, respectively. The vertical spacing of the range gates due to oversampling with 650 ns is 94 m. A summary of the technical specifications of the 482 MHz RWP is given in Table 1.

2.1.3 RS92-SGP radiosonde

The Vaisala RS92 radiosonde measures vertical profiles of pressure, temperature, and humidity from the ground up to the ballon bursting altitude limit of approximately 40 km. To retrieve the horizontal and meridional winds (u, v) based on the change of the sonde position, the RS92 is equipped with a GPS receiver. The noise in the raw u and v winds due to the radiosonde's pendulum and the noise of the GPS data is reduced by a low-pass digital filter (Dirksen et al., 2014). At Lindenberg, radiosondes are routinely launched four times a day at standard times (00:00, 06:00, 12:00, and 18:00 UTC). The temporal resolution of the sounding wind data is 40 s.

AMTD
7, 11439–11479, 2014

2.2 Doppler lidar data processing

The system output quantities relevant for the wind vector retrieval are the estimates of Doppler velocity $V_r(R, \alpha_i, t)$, where subscript i indicates the ith azimuth measurement within one VAD scan, and the corresponding signal-to-noise ratio SNR $= S/N$, where S is the average signal power and N the average noise power (Frehlich and Yadlowsky, 1994). The wind analysis is based on the following steps of data processing: (i) employment of SNR threshold technique for sorting out "bad" (noise affected) Doppler estimates from "good" estimates, (ii) calculation of 30 min average Doppler Lidar VAD scans to match the temporal resolution of the RWP measurements, (iii) reconstruction of the three vector components u, v, w, (iv) quality check to ensure consistency of retrieved winds and all the assumptions used in order to calculate u, v, w and (v) interpolation of the three vector components from the "Doppler lidar grid" to the "Wind profiler grid" to generate spatial matching. The latter step, however, is relevant for the final comparison between DL and RWP measurements and which otherwise would not have been necessary. Further details on the above described processing steps will be outlined below.

2.2.1 SNR thresholding technique

The measurable detector signal current in a DL is clearly affected by noise effects, mainly dominated by shot noise from the local oscillator (Frehlich and Kavaya, 1991; Frehlich, 1996). Since the systems operate down to very low SNR conditions, this leads to the occurrence of outliers in the signal properties estimation process ("bad" estimates), which are usually uniformly distributed in frequency over the Nyquist-limited search band (Dabas, 1999). In order to separate between "good" (reliable) and "bad" (unreliable) estimates, a simple SNR-based thresholding technique is a common approach. Depending on the instrument's specific parameters the SNR threshold may vary between different instruments. There are a number of studies focusing on techniques for the determination of reasonable threshold SNR, e.g. Frehlich and Yad-

AMTD
7, 11439–11479, 2014

lowsky (1994); Dabas (1999). For reliable Doppler velocity estimates with a precision of $< 30\,\mathrm{cm\,s^{-1}}$ the manufacturer of the StreamLine Doppler lidar suggests a threshold SNR of −18.2 dB (0.015). From test measurements during stable atmospheric conditions (vertical velocity close to zero), however, it turns out that this is a rather conservative value which is significantly limiting our data availability. In Fig. 2 the Doppler velocities measured during this test period are plotted against the corresponding value for SNR +1 (intensity). For the range $0.992 < (\mathrm{SNR} + 1) < 1.006$ the Doppler velocities are uniformly distributed over the search band indicating a relatively high fraction of "bad" estimates. Between the outer edge (SNR + 1 = 1.006) of the band of uniformly distributed Doppler and the proposed SNR threshold (SNR + 1 = 1.015), however, there is a large gap so that by employing this threshold SNR a huge amount of "good" measurements are discarded. Tests have shown, for instance, that the decrease of the threshold SNR from −18.2 dB (0.015) down to −20 dB (0.010) would increase the data availability by almost 40 %. However, since the goal of this paper was to assess the accuracy of strictly quality controlled DL wind measurements with respect to the RWP, a refinement of the SNR thresholding technique is left for a future study.

2.2.2 Calculation of 30 min averaged VAD scans

For the intercomparison of winds from the DL and the RWP it is necessary to achieve a match of the temporal resolution between both systems. The DL winds were therefore averaged to 30 min, which corresponds to the operational configuration of the RWP. Two different routes are available for this averaging: one option is to reconstruct first the cartesian vector components u, v, w from each single VAD scan which takes about 3 min (see also Sect. 2.1.1) and then to calculate averaged u, v, w vector components from ten full VAD scans. The other options is to average all VAD scans first and then to reconstruct the u, v, w wind vector components from these averaged VAD scans. Here the second way was used since it corresponds best to the "consensus averaging" method employed in the RWP processing.

AMTD
7, 11439–11479, 2014

2.2.3 Wind vector retrieval

The 3-D wind vector profiles are determined on the basis of the 30 min averaged VAD scans described above. Each averaged VAD scan includes temporally averaged Doppler velocities for 24 different directions. In principle, measurements in three linearly independent direction would be sufficient for a 3-D wind vector reconstruction. In this and the following sections (see Sect. 2.2.4), however, it will be shown that the use of VAD scans with more than three directions brings considerable benefits in terms of error minimization and in terms for conducting quality assurance of the reconstructed 3-D wind vector components, i.e. u, v, w.

Least squares wind components u, v, w using SVD:

Assuming a stationary and horizontally homogeneous wind field, i.e. $\boldsymbol{v}(x, y, z, t) \sim \boldsymbol{v}(z)$, the three wind vector components u, v and w can be obtained by solving the overdetermined linear system

$$\mathbf{A}\boldsymbol{v} = \boldsymbol{V}_r, \tag{1}$$

where $\boldsymbol{v} = (uvw)^{\mathrm{T}}$, $\boldsymbol{V}_r = (V_{r1}V_{r2}V_{r3}\ldots V_{rn})^{\mathrm{T}}$ (with $n = 360^\circ/15^\circ = 24$). The rows of matrix $\mathbf{A}$ are comprised of the unit vectors along the pointing directions (rays), that is

$$\mathbf{A} = \begin{pmatrix} \sin(\alpha_1)\sin(\phi) & \cos(\alpha_1)\sin(\phi) & \cos(\phi) \\ \sin(\alpha_2)\sin(\phi) & \cos(\alpha_2)\sin(\phi) & \cos(\phi) \\ \sin(\alpha_3)\sin(\phi) & \cos(\alpha_3)\sin(\phi) & \cos(\phi) \\ \ldots & \ldots & \ldots \\ \sin(\alpha_n)\sin(\phi) & \cos(\alpha_n)\sin(\phi) & \cos(\phi) \end{pmatrix}. \tag{2}$$

If the azimuth angle α_i (with $i = 1, \ldots, n$) and the zenith angle ϕ are chosen properly (see also Fig. 1), matrix $\mathbf{A}$ is a nonsquare 24×3 matrix with full column rank rank($\mathbf{A}$) = 3. Equation (1) is clearly overdetermined and can be solved using the method of least

AMTD
7, 11439–11479, 2014

squares. The solution is exact when it does exist, otherwise only an approximate solution can be found. A least squares solution $\boldsymbol{v}^*$ is obtained by minimizing the square of the residual in the 2-norm, i.e. by minimizing $\|\boldsymbol{V}_r - \mathbf{A}\boldsymbol{v}\|_2^2$ (e.g., Strang, 1993). In doing so the least squares solution is given by a standard square (3 × 3) system

$$\mathbf{A}^{\mathrm{T}}\mathbf{A}\,\boldsymbol{v} = \mathbf{A}^{\mathrm{T}}\boldsymbol{V}_r, \tag{3}$$

where $\mathbf{A}^{\mathrm{T}}$ is the transpose of $\mathbf{A}$. Since $\mathbf{A}$ has full column rank $\mathbf{A}^{\mathrm{T}}\mathbf{A}$ is positive definite and invertible, that is $\boldsymbol{v}$ can be obtained by evaluating the normal equation

$$\boldsymbol{v} = (\mathbf{A}^{\mathrm{T}}\mathbf{A})^{-1}\mathbf{A}^{\mathrm{T}}\boldsymbol{V}_r = \mathbf{A}^{+}\boldsymbol{V}_r, \tag{4}$$

where $\mathbf{A}^{+}$ denotes the Moore–Penrose Pseudoinverse of $\mathbf{A}$. The normal equations, however, tend to worsen the condition of the matrix, i.e. $\mathrm{cond}(\mathbf{A}^{\mathrm{T}}\mathbf{A}) = (\mathrm{cond}(\mathbf{A}))^2$. For a large condition number, small errors in the (measured) data can produce large errors in the solution. The singular value decomposition (SVD) can be used to solve least squares problem without squaring the condition of the matrix. Employing the SVD, the matrix $\mathbf{A}$ is decomposed using the factorization

$$\mathbf{A} = \mathbf{U}\mathbf{D}\mathbf{V}^{\mathrm{T}}, \tag{5}$$

where $\mathbf{U}$ is an 24 × 24 orthogonal matrix, $\mathbf{V}$ is an 3 × 3 orthogonal matrix and $\mathbf{D}$ is an 24 × 3 diagonal matrix whose elements are called the singular values of $\mathbf{A}$. Then a least squares solution can be expressed as

$$\boldsymbol{v} = \mathbf{A}^{+}\boldsymbol{V}_r = \mathbf{V}\mathbf{D}^{-1}\mathbf{U}^{\mathrm{T}}\boldsymbol{V}_r. \tag{6}$$

The advantage of using the SVD in the context of least squares minimization has also been discussed in Boccippio (1995).

AMTD
7, 11439–11479, 2014

Error propagation

Assuming that the Doppler velocity vector $\boldsymbol{V}_r$ has a corresponding known vector of uncertainty, i.e. $\boldsymbol{\sigma}_e = (\sigma_{e1}\sigma_{e2}\sigma_{e3}\ldots\sigma_{en})^{\mathrm{T}}$, the propagation of the radial velocity errors to the errors of the components of the wind vector $\boldsymbol{v}$ can be calculated employing the error propagation law. In matrix form, this can be written as

$$\mathbf{C}_{\boldsymbol{V}_r\boldsymbol{V}_r} = \mathbf{A}\mathbf{C}_{\boldsymbol{v}\boldsymbol{v}}\mathbf{A}^{\mathrm{T}} \tag{7}$$

or after rearranging to calculate the unknown uncertainties

$$\mathbf{C}_{\boldsymbol{v}\boldsymbol{v}} = \mathbf{A}^{-1}\mathbf{C}_{\boldsymbol{V}_r\boldsymbol{V}_r}(\mathbf{A}^{-1})^{\mathrm{T}}, \tag{8}$$

where $\mathbf{C}_{\boldsymbol{V}_r\boldsymbol{V}_r}$ and $\mathbf{C}_{\boldsymbol{v}\boldsymbol{v}}$ denote the variance-covariance matrices of $\boldsymbol{V}_r$ and $\boldsymbol{v}$ defined through the diagonal $n \times n$ matrix

$$\mathbf{C}_{\boldsymbol{V}_r\boldsymbol{V}_r} = \begin{pmatrix} \sigma_{e1}^2 & 0 & \ldots & 0 \\ 0 & \sigma_{e2}^2 & \ldots & 0 \\ \vdots & \vdots & \ddots & \vdots \\ 0 & 0 & \ldots & \sigma_{en}^2 \end{pmatrix} \tag{9}$$

and the 3×3 matrix

$$\mathbf{C}_{\boldsymbol{v}\boldsymbol{v}} = \begin{pmatrix} \sigma_u^2 & \sigma_{uv} & \sigma_{uw} \\ \sigma_{vu} & \sigma_v^2 & \sigma_{vw} \\ \sigma_{wu} & \sigma_{wv} & \sigma_w^2 \end{pmatrix}, \tag{10}$$

respectively. Here, the variance-covariance matrix $\mathbf{C}_{\boldsymbol{V}_r\boldsymbol{V}_r}$ is diagonal, because it is assumed that the errors of the n components of $\boldsymbol{V}_r$ are independent in different directions (Cohn and Goodrich, 2002). It has further been assumed that variances in the elevation angle occuring in $\mathbf{A}$ can be neglected. By evaluating the rhs of Eq. (8) the random

AMTD
7, 11439–11479, 2014

errors σ_u, σ_v and σ_w can be calculated from the square roots of the diagonal elements of the variance-covariance matrix $\mathbf{C_{vv}}$. For the more interested reader on the derivation of error propagation law in matrix form and its application reference is made to Arras (1998); Tellinghuisen (2001) and Boccippio (1995).

In the least square problem described above the measured radial velocities for each beam direction have a precision of $\sigma_{ei} < 30\,\mathrm{cm\,s^{-1}}$ with $i = 1, \ldots, n$ (see Sect. 2.2). Taking error propagation into account one obtains a precision of $\overline{\sigma}_{ei} < 10\,\mathrm{cm\,s^{-1}}$ for each beam direction from a full 30 min averaged VAD scan. Then, setting $\overline{\sigma}_{e1} \equiv \ldots \equiv \overline{\sigma}_{rn} \equiv \overline{\sigma}_e < 10\,\mathrm{cm\,s^{-1}}$ we find by evaluating Eq. (8) by means of SVD that

$$\mathbf{C_{vv}} = \begin{pmatrix} 124.4 & 1.9510^{-6} & 2.0110^{-7} \\ 1.9510^{-6} & 124.4 & -9.5510^{-7} \\ 2.01410^{-7} & -9.5510^{-7} & 4.465 \end{pmatrix}. \quad (11)$$

Eventually, calculating the square roots of the diagonal elements of $\mathbf{C_{vv}}$ yields

$$\sigma_u = \sigma_v < 11.15\,\mathrm{cm\,s^{-1}} \text{ and } \sigma_w < 2.11\,\mathrm{cm\,s^{-1}}. \quad (12)$$

Finally, the above described approach is used to study the variation of the retrieval uncertainties depending on the variation of the number of beam directions per VAD scan. Table 2 clearly shows that with increasing number of beam directions the uncertainties can be reduced, most obviously the uncertainty σ_w of the vertical wind component w. Thus it can be concluded, that a VAD scan is not only useful for horizontal wind vector reconstructions but also for the determination of the vertical wind provided the number of beam directions is high enough. Here, however, it should be kept in mind that the reconstructed w would differ from direct stare measurements because of the horizontal homogeneity assumption.

2.2.4 Quality assurance

The wind retrieval algorithm described in Sect. 2.2.3 is based on two assumptions. So far, the assumption of horizontal homogeneity has already been mentioned. This is

AMTD
7, 11439–11479, 2014

a necessary assumption to devise a closed set of equations for the unknown wind vector components u, v, w. The employment of regression techniques to obtain estimates for u, v and w presumes linear independence of the data set used for the retrieval, additionally. Wind retrievels from routinely DL measurements are thus only valid, if the real atmospheric conditions and the measurements meet these assumptions. In this section two parameters are described which have been used for conducting quality assurance of the retrieved winds.

Test of horizontal homogeneity

It is well known that the wind field is not always horizontally homogeneous, this is mainly due to convection, gravity waves or shear induced turbulence. Characteristic temporal and spatial scales for turbulence are $T = 10$ s and $L = 1$ m. For thermally induced convective processes we typically have $T = 5$ min and $L = 500$ m. Thus, with reference to a full DL scan lasting about 3 min and with a scannnig circle having height dependent diameters d_C of about $d_C \sim 300$ m at an altitude of ~ 550 m and $d_C \sim 5360$ m at ~ 10 km it is often the case that due to the occurrence of turbulent motions there are rapid wind fluctuations along the scanning circle and accordingly the assumption of a horizontally homogeneous wind field is not fulfilled. For that reason 3-D wind vector retrievals based on measurements collected during such inhomogeneous wind field conditions have to be flagged. The strategy used to identify wind retrievals during such inhomgeneous wind field conditions is described next.

For a horizontally homogeneous wind field, the reconstruction of the mean wind u, v, w from radial velocities obtained by a VAD scan scheme can be regarded as a sine wave fitting (Banakh and Smalikho, 2013). The overall quality of the fit to this sine wave model is affected by deviations from these homogeneous conditions and can be measured by the coefficient of determination R^2 defined through

$$R^2 = 1 - \sum_i (V_{ri} - \widetilde{V}_{ri})^2 \Big/ \sum_i (V_{ri} - \overline{V}_r)^2 , \quad (13)$$

AMTD
7, 11439–11479, 2014

with $\overline{V}_r = \sum_i V_{ri}$ and $\widetilde{V}_{ri}$ denoting the radial velocities from the "sine wave fit". R^2 is used as a quality control parameter for u, v and w reconstructions.

For the analysis in the present paper a reconstructed 3-D wind vector has been rejected if $R^2 < 0.95$. An interpretation of this value is that 95 % of the variations of the averaged VAD scan Doppler velocities are due to variations in the beam direction α_i and only 5 % of the variations have to be explained by other factors. For an exact horizontally homogeneous wind field and exact Doppler velocity estimates the VAD Doppler velocity variations are solely caused by the variation in the beam direction α_i. Thus, with the requirement $R^2 < 0.95$ it is possible to identify such VAD scans for which the assumption of a horizontal wind field is only partially fulfilled.

Collinearity diagnostics

Following the strategy described above it was found, however, that $R^2 \geq 0.95$ can only be regarded as a necessary condition for "good" reconstructions. A sufficient condition is that the degree of collinearity among the Doppler velocity measurements used for the retrieval is relatively weak, since linear independence of the sampling directions is an essential prerequisite for the reconstruction of the wind vector. Multicollinearity describes a high linear relationship among one or more independent variables (Belsley et al., 1980) and it is a well known issue in regression analysis that multicollinearity may result in parameter estimates with incorrect signs and implausible magnitudes (Mela and Kopalle, 2002) or may affect the regressions robustness, i.e. small changes in the data may result in large changes in the parameter estimates (Boccippio, 1995). Thus, multicollinearity makes the parameter estimates less reliable and has to be detected to exclude erroneous (unphysical) u, v, w retrievals from VAD scans. In the context of least squares parameter estimation from a VAD scan, a high degree of multicollinearity may occur in situations when there are large azimuthal gaps in the measurements due to limited or non-existing backscattering targets within the atmosphere. Then, one measured Doppler velocity can be linearly predicted from the neighboring values and

AMTD
7, 11439–11479, 2014

thus the available measurements from such an "incomplete" scan contain redundant information on the wind field and it becomes difficult or impossible to distinguish their individual influences on the u, v and w estimates. This issue was already recognized by Matejka and Srivastava (1991) from the VAD analysis of single-Doppler Radar Data.

The condition number CN is a parameter that can be used for the detection of collinearity. If the condition number of the problem is small (close to 1) the degree of collinearity is relatively weak. In contrast, a large condition number is an indicator for a strong collinearity among the variables. Boccippio (1995) employed the condition number for an analysis of the VVP (volume velocity processing) retrieval method and identified condition numbers around 9–12 as a threshold indicating collinearity in the regression. In Wissman et al. (2007) values for CN of 10 and 30 are mentioned to indicate medium and serious degrees of multicollinearity, respectively.

For the collinearity diagnostics the approach as described in Boccippio (1995) has been adopted. In particular, CN is calculated based on the standardized (scaled) data matrix $\mathbf{Z} = \mathbf{AS}$, where

$$\mathbf{S} = \mathrm{diag}(s_1, s_2, s_3) \text{ with } s_i = \left(\boldsymbol{A}_i^{\mathrm{T}} \boldsymbol{A}_i\right)^{-1/2}. \tag{14}$$

Here, $\boldsymbol{A}_i$ denote the columns of matrix $\mathbf{A}$, i.e. $\mathbf{A} = [\boldsymbol{A}_1 \boldsymbol{A}_2 \boldsymbol{A}_3]$. If the singular value decomposition of $\mathbf{Z}$ is used, the condition number CN($\mathbf{Z}$) can be calculated as

$$\mathrm{CN}(\mathbf{Z}) = \frac{\eta_{\max}}{\eta_{\min}}, \tag{15}$$

where η_i ($i = 1, 2, 3$) are the singular values of $\mathbf{Z}$. The standardization of the data matrix is recommendend by Belsley (1991). For further details concerning the scaling problem of the condition number it is also referred to Wissman et al. (2007). Figure 3 indicates an increase of the condition number with increasing azimuthal gaps for a VAD scan configuration. For a gap size of 270° the condition number is CN = 30 which according to Wissman et al. (2007) indicates severe collinearity. In such a case, all radial measurements stem from only one quadrant of the scan. Geometrically it is obvious

AMTD
7, 11439–11479, 2014

that the linear independence in this case is numerically weak. For the quality control used in the present analysis a CN threshold of 10 has been used which means that 3-D wind vector reconstructions obtained from VAD scans with azimuthal gaps $\geq 240^\circ$ have been rejected.

Example

An example for the outcome of the above described strategy of quality control is illustrated in Fig. 4. The 30 min averaged wind profiles shown here are based on DL measurements from 22 August 2013, which was a typical summer day with a pronounced diurnal cycle of a convective boundary layer (CBL). The plots in the left column show unverified 30 min averaged vertical profiles of wind speed and wind direction, respectively. The plots in the right column show the corresponding wind profiles after consistency checking. The parameters R^2 and CN are shown in Fig. 5. The processing was done as described in Sect. 2.2.3. Appendix A provides guidance for the calculation of wind speed and wind direction from u, v, w retrievals, additionally. It can be observed that profiles between 08:00 UTC and 14:00 UTC were rejected. This is mainly due to values for $R^2 < 0.95$ which can be attributed to the inhomogeneous flow occurring within a well established CBL. Figure 6 illustrates this situation by showing VAD fits for both homogeneous and inhomogeneous situations.

With regard to the condition number, Fig. 5 shows only a few cases with CN > 10, most in the upper part of the boundary layer where azimuthal gaps within the VAD scan are more likely due to absence of backscattering targets. Even if multicollinearity is a rare problem there is a need to define a CN threshold (here CN > 10) as a sufficient condition. This can be motivated based on the examples shown in Fig. 7. Three VAD scans obtained between 11:03 UTC and 11:32 UTC for three adjacent range gate heights at $h_1 = 1460,48$ m, $h_2 = 1506,84$ m and $h_3 = 1553,21$ m are shown along with the corresponding consistency check parameters R^2 and CN. Obviously, the sine wave fit at h_3 has a much greater amplitude compared to h_2 and h_1. Since the amplitude is a measure for the wind speed, this would imply much stronger winds at h_3 than at the

AMTD
7, 11439–11479, 2014

lower heights at h_2 and h_1. The condition number of CN = 22 clearly reflects the large gap of radial velocity measurements between the azimuth angles 50 and 300°. The high degree of collinearity among the Doppler velocities for this VAD scan is obviously leading to erroneous magnitudes for the parameter estimates u, v and w.

In summary, the parameters R^2 and CN turn out to be useful quality control indicators for the 3-D wind vector retrieval although they apparently do not detect all "bad" winds. In Fig. 4 the plot of the quality flagged wind speed still includes in 12th position a profile whose values does not seem to fit into the overall wind speed pattern despite the good quality check parameters R^2 = 0.98 and CN = 3. It remains for future work to analyse the error sources for this type of possibly wrong wind retrieval.

2.2.5 Regridding

The Doppler lidar measurements obtained with our configurations have a vertically finer resolution than the measurements of the RWP. For the purpose of intercomparisons between Doppler lidar-, RWP and radiosonde measurements it is therefore useful to define a common reference grid to make the values comparable. Since the interpolation from a coarser grid to a finer grid is naturally more problematic than vice versa, we have chosen the wind radar grid as the reference grid for our studies. For the interpolation of the 30 min averaged 3-D wind vector components u, v, w from the finer Doppler lidar (or finer Radiosonde) grid to the coarser and equidistant grid of the RWP, a cubic spline interpolation was used. In detail this means that between two grid points of the finer grid we first determined a smooth function which passes exactly through those points. Between two grid points of the finer grid, the smooth function is evaluated at the coarser grid point to get the interpolated value.

AMTD
7, 11439–11479, 2014

3 Analysis/statistics

In this section the statistics of one-year long DL measurements for wind speed and wind direction is presented. A guidance for the calculation of wind speed and direction from the u, v, w retrievals is provided in Appendix A. The results are verified with corresponding measurements obtained with a collocated 482 MHz RWP and measurements from RS92-SGP Radiosonde launched at the same observation site.

3.1 Data availability

For the period under investigation, the maximum number of 30 min averaged profiles for wind speed and wind direction is 17 568 provided the measurement conditions are perfect, i.e. occurrence of aerosols and/or cloud droplets at any time and any height during the year of measurements. Clearly, measurement conditions are not always ideal as shown in Fig. 8 which naturally leads to a decrease in the number of quality controlled data. At the lowest level of the reference grid (i.e. 552 m) a total of 9798 (∼ 56 %) averaged values could be obtained whereas these numbers decrease to 697 (∼ 4 %) at 2056 m. The decrease of data availability continues further upwards and approaches less than 10 (∼ 0.06 %) for altitudes higher than 7038 m. This strong decrease of data availability reflects the nature of the aerosol and cloud particle concentration within the atmosphere. This is the main reason why the IR Doppler lidar is mainly used for wind measurements within the ABL.

Also shown in Fig. 8 is the data availability obtained with the collocated RWP (low mode) and those from routine RS launches. Not surprisingly, both measurement systems provide higher data availabilities within the free atmosphere than the DL. The decrease of RWP data availability with height is related to the profile of the structure constant of refractive index turbulence (C_n^2) which can be observed almost continously in the lower atmosphere (Atlas, 1990). For the two comparisons, i.e. Doppler lidar vs. RWP (hereafter referred to as DLWR) and Doppler lidar vs. radiosonde (hereafter referred to as DLRS), we only use the subset where valid data are available from both

AMTD
7, 11439–11479, 2014

systems, i.e. the intersection of the respective data sets. Figure 8 gives an overview to what extent this further decreases the data availability for our statistical analysis. To get almost representative statistical results for a "one-year comparison" the comparisons are restricted to heights up to ~ 2800 m for the comparison DLWR and up to ~ 1300 m for the comparison DLRS, which guarantees that the sample size is > 200. For this data basis the precision $\Delta\overline{v}_{\mathrm{speed}}$ of a calculated quasi-annual wind speed is on the order of about $\Delta\overline{v}_{\mathrm{speed}} = 7 \times 10^{-4}\,\mathrm{m\,s^{-1}}$ (see also Appendix B).

3.2 DLWR and DLRS comparisons

For a first overview, the 30 min averaged lidar winds are compared against 30 min averaged RWP winds on the one hand and against temporally consistent radiosonde winds on the other hand for the full period and all heights. The corresponding scatter plots are shown in Fig. 9 for wind speed and wind direction, respectively. Regarding the wind speed it can be observed that for both comparisons (DLWR and DLRS) a great fraction of the data sets falls on the identity line which indicates a general good agreement of the respective data samples. In more detail, however, the correlation (m) indicates a slight better linear relationship between radiosonde and Doppler lidar wind speeds (m = 0.99) than between RWP and Doppler lidar wind speeds (m = 0.97). This seems to be mainly due to better agreements of higher wind speeds (e.g. $> 20\,\mathrm{m\,s^{-1}}$) for the DLRS comparison than for the DLWR comparison.

Additionally we observe a greater spread of data pairs around the identity line for the DLWR comparison than for the DLRS comparison. However, the respective RMSE scores which measure the average magnitude of the error indicate better agreement for the DLWR comparison than for the DLRS comparison. Since the RMSE gives a high weight to large errors, the lower RMSE value for the DLWR comparison also indicates that the largest differences occur between the Doppler Lidar and Radiosonde data. Regarding the wind direction the dots of a huge number of data pairs are concentrated around the identity line and thus likewise indicate good agreements for both compar-

AMTD
7, 11439–11479, 2014

isons. However, the dots of some minor data pairs are somewhat widely spread and indicate a weak relationship between measured wind directions. We also find that this observation is more pronounced for the DLWR comparison than for the DLRS comparison. Note that the clustered data points around 360° at both the horizontal and vertical axis are due to the cyclic azimuth range.

A general good agreement in the statistics of Doppler Lidar-, Radar Wind Profiler- and Radiosonde measurements is also reflected in the annual mean of the measured vertical profiles for wind speed and direction shown in Fig. 10. To quantify the errors, the following verification scores are analyzed: mean error (ME), mean absolute error (MAE) and root mean squared error (RMSE). Regarding the DLWR comparison the ME for the wind speed changes a little in sign with varying height up to about 1800 m, whereas the range of speed variations is from $-0.2\,\mathrm{m\,s^{-1}} < \mathrm{ME} < 0.3\,\mathrm{m\,s^{-1}}$. Above 1800 m the ME is always positive and increases from $\sim 0\,\mathrm{m\,s^{-1}}$ at 1800 m up to $0.2\,\mathrm{m\,s^{-1}}$ at about 2500 m. Thus, assuming that the RWP measures the "truth" a systematic error indicating a slight overestimation of Doppler Lidar wind speeds can be identified for altitudes higher than 1800 m. Concerning the annual mean wind direction there is in general also good agreement between DL and RWP measurements. Here the mean differences mostly vary between ±1°. For MAE and RMSE, the DL and RWP measurements agree in wind speeds mostly within a range of about $0.3\,\mathrm{m\,s^{-1}} < \mathrm{MAE} < 0.5\,\mathrm{m\,s^{-1}}$ and $0.5\,\mathrm{m\,s^{-1}} < \mathrm{RMSE} < 0.7\,\mathrm{m\,s^{-1}}$. For the wind direction $3^\circ < \mathrm{MAE} < 4^\circ$ and $5^\circ < \mathrm{RMSE} < 10^\circ$. The small differences between the MAE and RMSE ranges for the wind speed additionally indicate that there is some variation in the magnitude of the errors but large errors can be ruled out in all likelihood. This is in contrast to the slightly larger differences between the MAE and RMSE ranges for the wind direction at low range gate heights, suggesting that here larger errors occur. Regarding the DLRS comparison we observe a smaller bias ($-0.2\,\mathrm{m\,s^{-1}} < \mathrm{ME} < 0.1\,\mathrm{m\,s^{-1}}$) below 1500 m than in the DLWR comparison. The verification scores MAE and RMSE, however, are somewhat larger, i.e. $0.5\,\mathrm{m\,s^{-1}} < \mathrm{MAE} < 0.7\,\mathrm{m\,s^{-1}}$ and

AMTD
7, 11439–11479, 2014

$0.7\,m\,s^{-1} < RMSE < 0.9\,m\,s^{-1}$ for wind speed and $5^\circ < MAE < 6^\circ$ and $9^\circ < RMSE < 12^\circ$ for wind direction.

The presented long-term intercomparison results confirm the main findings of previous intercomparison results (see Sect. 1) obtained from short-term measurement periods. The good agreement also indicates a rather small instrument error of all systems, since the methodology of the comparison was targeted at minimizing the sampling error by minimizing of both the temporal and spatial separation (about 30 m) between the Doppler lidar and the radar wind profiler.

4 Range aliasing effects for smaller SNR thresholds

In Sect. 2.2.1 it has already been mentioned that the SNR threshold of −18.2 dB (1.015) used for the analysis in the present paper is a rather conservative threshold, with the consequence that a huge amount of "good" estimates are rejected. It can therefore be assumed that smaller SNR-thresholds can possibly also be used. An analysis of the Doppler lidar measurements based on an SNR threshold < 1.015 revealed an interesting type of "gross error", which was not observed employing the conservative SNR threshold = 1.015. In radar meteorology, this type of "gross error" is already well known as range ambiguity (or range aliasing). Range aliasing occurs if there are atmospheric backscattering targets at altitudes $> Z_{max}$, where Z_{max} defines the greatest unambiguous measurement height specified through the pulse repetition frequency (PRF) via $PRF_{max} = c/(2Z_{max})$. Here, c defines the speed of light. In such a case an incorrect calculation of the range of the backscattering target is unavoidable, since the received echo and the outgoing pulse are assigned to each other incorrectly: the received signal is not associated with the pulse just transmitted, but with the pulse transmitted prior to the latest one. The wind profiles shown in Fig. 12 give an example where such range aliasing effects have been detected by comparing Doppler lidar measurements with RWP measurements. It is important to point out that such "gross errors" can be circum-

AMTD
7, 11439–11479, 2014

vented by changing the PRF in the sense that the maximum unambiguous sampling range is increased.

5 Conclusions

The capability of a new generation of portable IR Doppler lidar systems for future operational boundary layer wind profiling, complementary to radar profilers, has been tested. For this purpose, one year long times series of horizontal wind vector retrievals from Doppler lidar and radar wind profiler measurements of Doppler velocity have been compared mainly for atmospheric boundary layer heights between 500 and 2800 m. These interval limits coincide with the lower limit for 482 MHz wind profiler measurements and an upper limit up to which nearly continous Doppler lidar measurements were possible. The higher limit is a representative value for the RAO site and is subject to natural conditions as the atmospheric aerosol loading at this site. There is a general good agreement in the measurement statistics of both systems and thus confirms previous studies on this issue but on the basis of a much smaller data collection. These results strengthen the basic idea to use DL measurements below 500 m to fill the gap below 500 m in the wind profiles where 482 MHz RWP wind measurements are no more possible.

The underlying assumptions used for the 3-D wind vector retrievals from Doppler velocity measurements have been the same for both systems. A huge advantage of the Doppler Lidar, however, is that the full hemispheric scanning capability of the DL allows for more flexible sampling strategies than the RWP which is restricted to measurements using the DBS mode. In this context it became apparent that DL measurements based on a VAD scan with $n = 24$ beam directions enable additional quality checks to ensure consistency of retrieved winds and retrieval assumptions. In particular, if the number of measurement directions (n) is large enough the "Goodness-of-fit" parameter quantified by R^2 turned out to be a useful tool to determine the degree of homogeneity of the wind field during the time at which measurement data have been collected. Inhomoge-

AMTD
7, 11439–11479, 2014

neous wind fields are more characteristic within the atmospheric boundary layer than in the free atmosphere. That is why such a consistency check is more important for wind retrievals within the boundary layer than in the free atmosphere. The R^2 quality test employed discards a considerable proportion of DL wind retrievals when the wind field is non-homogeneous. This is justified because the focus of the investigation was the evaluation of strictly quality controlled wind measurements of the DL. By the same token, the SNR threshold was also chosen in a very conservative way. It remains for future work to find out to what extent these constraints can be relaxed for the sake of a higher data availability without compromising the data quality of the measurements. A further test of linear independence among the Doppler velocity measurements by means of the condition number CN turned out to be useful to detect physically implausible retrievals which may have its origin in large measurement gaps within a single VAD scan. This can be the case if the backscattering targets are inhomogeneously distributed which frequently occurs within the transition zone from the atmospheric boundary layer into the free atmosphere. The results of the employment of the two test parameters R^2 and CN presented in this study make clear the importance of quality assurance testing and it is understood that the strategy of quality assurance testing employed here was important for the good agreements between Doppler lidar and radar wind profiler measurements.

Appendix A: Wind speed and wind direction

From the 3-D wind vector components u, v, w we calculate the horizontal wind speed (v_{speed}) and wind direction (Dir) via

$$v_{\text{speed}} = \sqrt{u^2 + v^2}, \tag{A1}$$

AMTD
7, 11439–11479, 2014

and

$$\mathrm{Dir} = \begin{cases} 270^\circ - \arctan(v/u)(180^\circ/\pi) & \text{if } u > 0 \\ 90^\circ - \arctan(v/u)(180^\circ/\pi) & \text{if } u < 0 \\ 180^\circ & \text{if } u = 0, v > 0 \\ 360^\circ & \text{if } u = 0, v < 0. \end{cases} \quad \text{(A2)}$$

To compute the precision of the estimates v_{speed} and Dir we use the Gaussian error propagation

$$\sigma_{\mathrm{speed}} = \sqrt{\left(\frac{\partial v_{\mathrm{speed}}}{\partial u}\sigma_u\right)^2 + \left(\frac{\partial v_{\mathrm{speed}}}{\partial v}\sigma_v\right)^2} \quad \text{(A3)}$$

$$\sigma_{\mathrm{Dir}} = \sqrt{\left(\frac{\partial \mathrm{Dir}}{\partial u}\sigma_u\right)^2 + \left(\frac{\partial \mathrm{Dir}}{\partial v}\sigma_v\right)^2} \quad . \quad \text{(A4)}$$

Appendix B: Error propagation

Suppose $\overline{v}_{\mathrm{speed}}$ is an averaged value defined through $\overline{v}_{\mathrm{speed}} = 1/N \sum_{i=1}^{N} v_{\mathrm{speed},i}$ and where the $v_{\mathrm{speed},i}$'s are single wind speed values. Then the error $\Delta\overline{v}_{\mathrm{speed}}$ of the averaged value $\overline{v}_{\mathrm{speed}}$ is given by

$$\Delta\overline{v}_{\mathrm{speed}} = (1/N)\sqrt{\sum_{i=1}^{N}(\Delta v_{\mathrm{speed},i})^2}, \quad \text{(B1)}$$

where $\Delta v_{\mathrm{speed},i}$ are the errors of $v_{\mathrm{speed},i}$, respectively.

AMTD
7, 11439–11479, 2014

It can be shown that by use of $\sigma_u = \sigma_v$ (see Eq. 12) from Eq. (A3) can be concluded that

$$\sigma_u = \sigma_v = \sigma_{\text{speed}} = 0.0095\,\text{m}\,\text{s}^{-1}. \quad \text{(B2)}$$

Provided that measurements for all 24 beam directions have been available σ_{speed} can be regarded as a general value for an upper bound of the precision. Then, using

$$\sigma_{\text{speed}} = \Delta v_{\text{speed},1} = \Delta v_{\text{speed},2} = \ldots = \Delta v_{\text{speed},N}, \quad \text{(B3)}$$

Eq. (B1) simplifies to

$$\Delta\bar{v}_{\text{speed}} = (1/N)\sqrt{N \cdot (\sigma_{\text{speed}})^2} \quad \text{(B4)}$$

Acknowledgements. This work was carried out as part of the HD(CP)^2 project (sub-project: "O1 – supersites") funded by the German Federal Ministry of Education and research (BMBF) – grant number 01LK1209E. The authors would like to acknowledge METEK GmbH for its support during the installation and use of the "StreamLine" Doppler Lidar system. We are also grateful to Guy Pearson for comments on an earlier version of the manuscript.

The service charges for this open access publication have been covered by Deutscher Wetterdienst (DWD).

References

Arras, K. O.: An Introduction to Error Propagation: Derivation, Meaning and Examples of Equation $C_Y = F_X C_X F_X^T$, ETH-Zürich, Technical Report No. EPFL-ASL-TR-98-01 R3, doi:10.3929/ethz-a-010113668 (last access: 11 November 2014), 1998. 11450

Atlas, D.: Radar in Meteorology, American Meteorological Society, 45 Beacon Street, Boston, MA, 02176, 1990. 11456

Banakh, V. and Smalikho, I.: Coherent Doppler Wind Lidars in a Turbulent Atmosphere, Publishers, Printed and bound in the United States of Amerika, 2013. 11451

AMTD
7, 11439–11479, 2014

Belsley, D.: A guide to using the collinearity diagnostics, Computer Science in Economics and Management, 4, 33–50, 1991. 11453
Belsley, D., Kuh, E., and Welsch, R. E.: Regression Diagnostics: Identifying Influential Data and Sources of Collinearity, John Wiley & Sons, Inc., Hoboken, New Jersey, 1980. 11452
Boccippio, D. J.: A diagnostic analysis of the VVP single-doppler retrieval technique, J. Atmos. Ocean. Tech., 12, 230–248, doi:10.1175/1520-0426(1995)012<0230:ADAOTV>2.0.CO;2, 1995. 11448, 11450, 11452, 11453
Cohn, S. A. and Goodrich, R. K.: Radar wind profiler radial velocity: a comparison with Doppler lidar, J. Appl. Meteorol., 41, 1277–1282, 2002. 11441, 11449
Dabas, A.: Semiempirical model for the reliability of a matched filter frequency estimator for Doppler lidar, J. Atmos. Ocean. Tech., 16, 19–28, doi:10.1175/1520-0426(1999)016<0019:SMFTRO>2.0.CO;2, 1999. 11445, 11446
Dirksen, R. J., Sommer, M., Immler, F. J., Hurst, D. F., Kivi, R., and Vömel, H.: Reference quality upper-air measurements: GRUAN data processing for the Vaisala RS92 radiosonde, Atmos. Meas. Tech. Discuss., 7, 3727–3800, doi:10.5194/amtd-7-3727-2014, 2014. 11444
Fischler, M. A. and Bolles, R. C.: Random sample consensus: a paradigm for model fitting with applications to image analysis and automated cartography, Commun. ACM, 24, 381–395, 1981. 11444
Frehlich, R.: Simulation of coherent Doppler lidar performance in the weak-signal regime, J. Atmos. Ocean. Tech., 13, 646–658, doi:10.1175/1520-0426(1996)013<0646:SOCDLP>2.0.CO;2, 1996. 11445
Frehlich, R. G. and Kavaya, M. J.: Coherent laser radar performance for general atmospheric refractive turbulence, Appl. Optics, 30, 5325–5352, doi:10.1364/AO.30.005325, 1991. 11445
Frehlich, R. and Yadlowsky, M.: Performance of mean-frequency estimators for Doppler radar and lidar, J. Atmos. Ocean. Tech., 11, 1217–1230, 1994. 11444, 11445
Matejka, T. and Srivastava, R. C.: An improved version of the extended velocity-azimuth display analysis of single-doppler radar data, J. Atmos. Ocean. Tech., 8, 453–466, doi:10.1175/1520-0426(1991)008<0453:AIVOTE>2.0.CO;2, 1991. 11453
Mela, C. and Kopalle, P.: The impact of collinearity on regression analysis: the asymmetric effect of negative and positive correlations, Appl. Econ., 34, 667–677, 2002. 11452
Pearson, G., Davies, F., and Collier, C.: An analysis of the performance of the UFAM pulsed Doppler lidar for observing the boundary layer, J. Atmos. Ocean. Tech., 26, 240–250, doi:10.1175/2008JTECHA1128.1, 2009. 11441

AMTD
7, 11439–11479, 2014

Shaw, W., Darby, L., and Banta, R.: A comparison of winds measured by a 915 MHz wind profiling radar and a Doppler lidar, 83rd AMS annual meeting (12th Symp. on Met. Observ. & Instrument.), Long Beach, CA, 9-13 February, P1.8, https://ams.confex.com/ams/pdfpapers/58646.pdf (last access: 11 November 2014), 2003. 11441

Strang, G.: The fundamental theorem of linear algebra, Am. Math. Mon., 100, 848–855, 1993. 11448

Strauch, R. G., Merritt, D. A., Moran, K. P., Earnshaw, K. B., and van de Kamp, D.: The Colorado wind profiling network, J. Atmos. Ocean. Tech., 1, 37–49, 1984. 11444

Tellinghuisen, J.: Statistical error propagation, J. Phys. Chem. A, 105, 3917–3921, doi:10.1021/jp003484u, 2001. 11450

Wissman, M., Toutenburg, H., and Shalabh: Role of Categorical Variables in Multicollinearity in the Linear Regression Model, Tech. Rep. Number 008, Department of Statistics, University of Munich, Germany, Technical Report Number 008, 34 pp., http://nbn-resolving.de/urn/resolver.pl?urn=nbn:de:bvb:19-epub-2081-0 (last access: 11 November 2014), 2007. 11453

AMTD
7, 11439–11479, 2014

Table 1. Parameters of the HALO Photonics StreamLine Doppler lidar and the Vaisala/Rohde&Schwarz 482 MHz wind profiler (LAP-16000) installed at the observation site RAO. During the measurement period from 2 October 2012 to 2 October 2013 the two operating parameters (1) total number of pulses averaged and (2) resolution of Doppler velocity have been changed. The values in the brackets are valid starting from 26 July 2013.

	Doppler lidar	Radar wind profiler
wavelength	1.5 µm	62 cm
pulse width	160 ns	1000 ns
range gate length	48 m	94 m
points per range gate	16	1
total number of range gates	200	96
total number of pulses averaged	75 000	507 904 (491 520)
resolution of Doppler velocity	$\pm 0.0382\,m\,s^{-1}$	0.1195 (0.1250)
telescope focus	800 m	not applicable
pulse length	25 m	150 m
total observation time per range gate	320 ns	650 ns
sampling frequency	50 MHz	1.538 MHz
Nyquist velocity	$\pm 19.4\,m\,s^{-1}$	$30.586\ (31.996)\,m\,s^{-1}$
number of FFT points	1024	512
pulse repetition frequency (PRF)	15 kHz	12.195 (12.346) kHz

AMTD
7, 11439–11479, 2014

Table 2. Decrease of the uncertainties ($\sigma_u, \sigma_v, \sigma_w$) in the 3-D wind vector component retrievals u, v and w with increasing number n of equidistant beam directions per VAD-scan. The values are calculated via Eq. (8) assuming a Doppler velocity uncertainty of $\sigma_r = 10\,\mathrm{cm\,s^{-1}}$ for each beam direction. $\Delta\alpha$ indicates the azimuth resolution.

n	$\Delta\alpha$ [°]	$\sigma_u = \sigma_v$ [$\mathrm{cm\,s^{-1}}$]	σ_w [$\mathrm{cm\,s^{-1}}$]
3	120	31.5470	5.97717
4	90	27.3205	5.17638
6	60	22.3071	4.22650
12	30	15.7735	2.98858
18	20	12.8790	2.44017
24	15	11.1536	2.11325
36	10	9.10684	1.72546

AMTD
7, 11439–11479, 2014

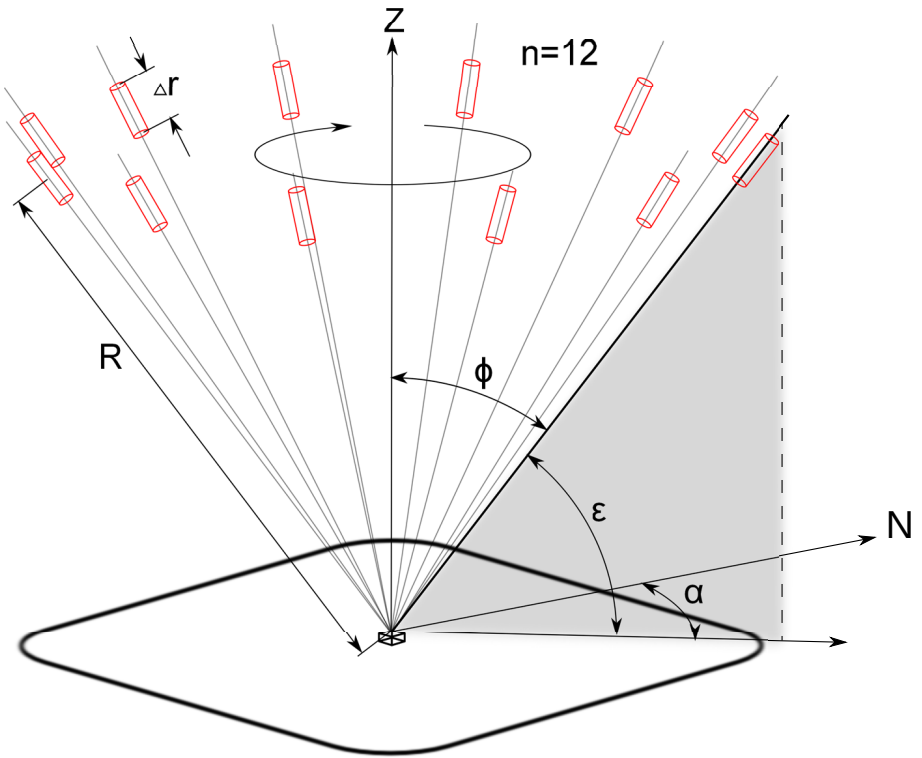

Figure 1. Example for a velocity-azimuth display (VAD) scanning technique for $n = 12$ beam directions. The laser beam of the Doppler Lidar points upwards with a constant elevation angle ε and rotates around the vertical Z with configurable azimuth angles α. The red volumes symbolize an emitted "light"-disturbance of a specified period of time (i.e. pulse width Δt) travelling along the line-of-sight (LOS). R is the range of the measurement along LOS and Δr defines the pulse length. The latter is related to the pulse width via $\Delta r = c \cdot \Delta t/2$, with c denoting the speed of light.

AMTD
7, 11439–11479, 2014

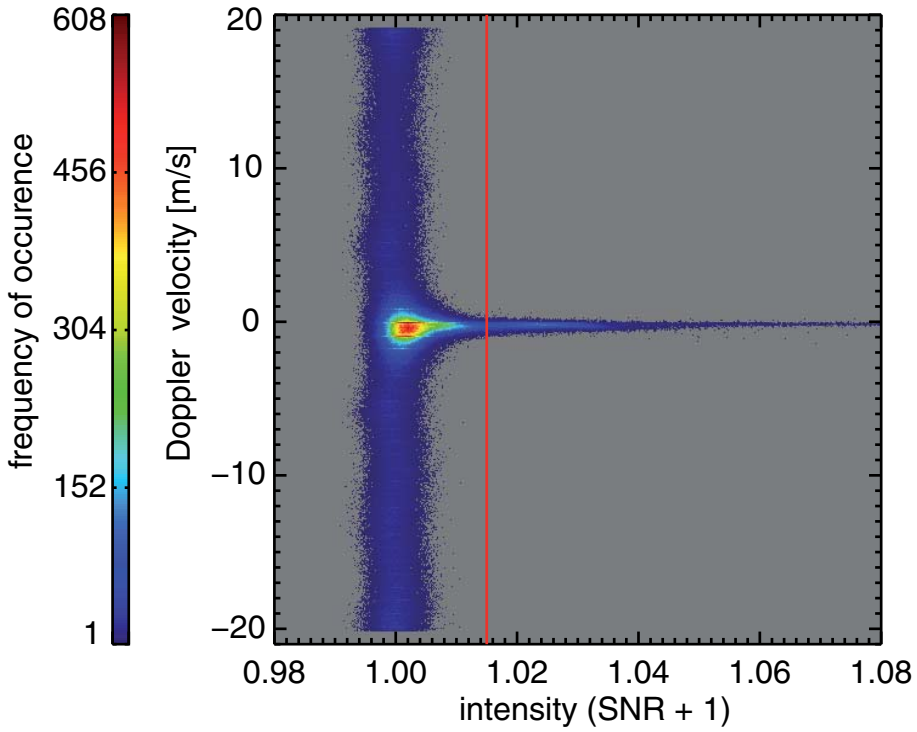

Figure 2. Intensity (SNR + 1) vs. Doppler velocity from two measurement periods during stable atmospheric conditions (06:00–07:00 UTC 5 July 2013 and 07:00–08:00 UTC 22 July 2013) with vertical velocities close to zero. For the range $0.992 < (\mathrm{SNR} + 1) < 1.006$ the Doppler velocities are uniformly distributed over the search band ($\pm 19.4\,\mathrm{m\,s^{-1}}$) indicating a relatively high fraction of "bad" estimates. For $\mathrm{SNR} + 1 \geq 1.006$ the Doppler lidar delivers plausible values ("good" estimates). The red line indicates the SNR-threshold (SNR + 1) = 1.015 used for the data analysis in the present paper.

AMTD
7, 11439–11479, 2014

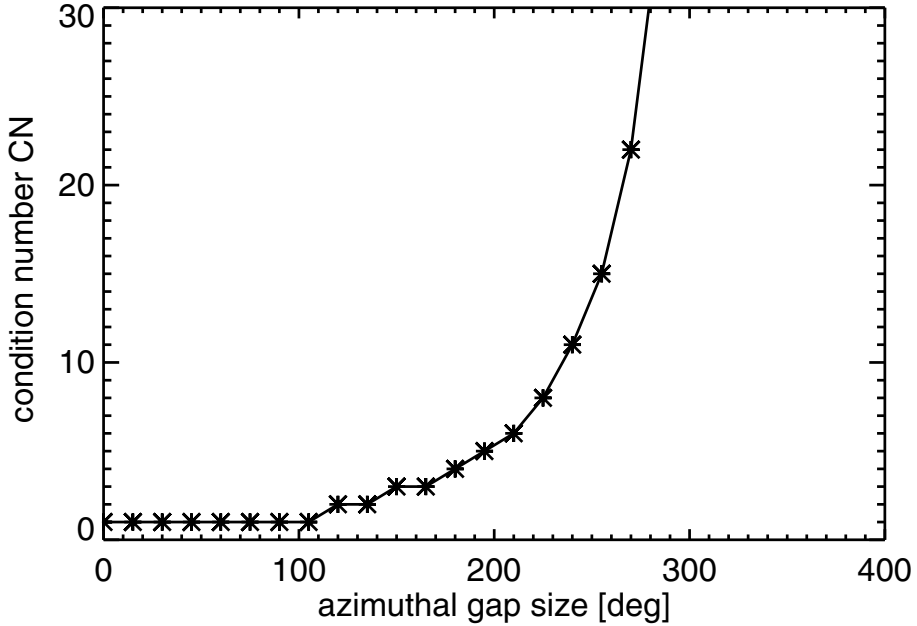

Figure 3. Condition number (CN) vs. azimuthal gap size for a VAD scan with 15° intervals of azimuth α and a constant elevation angle $\varepsilon = 75°$.

AMTD
7, 11439–11479, 2014

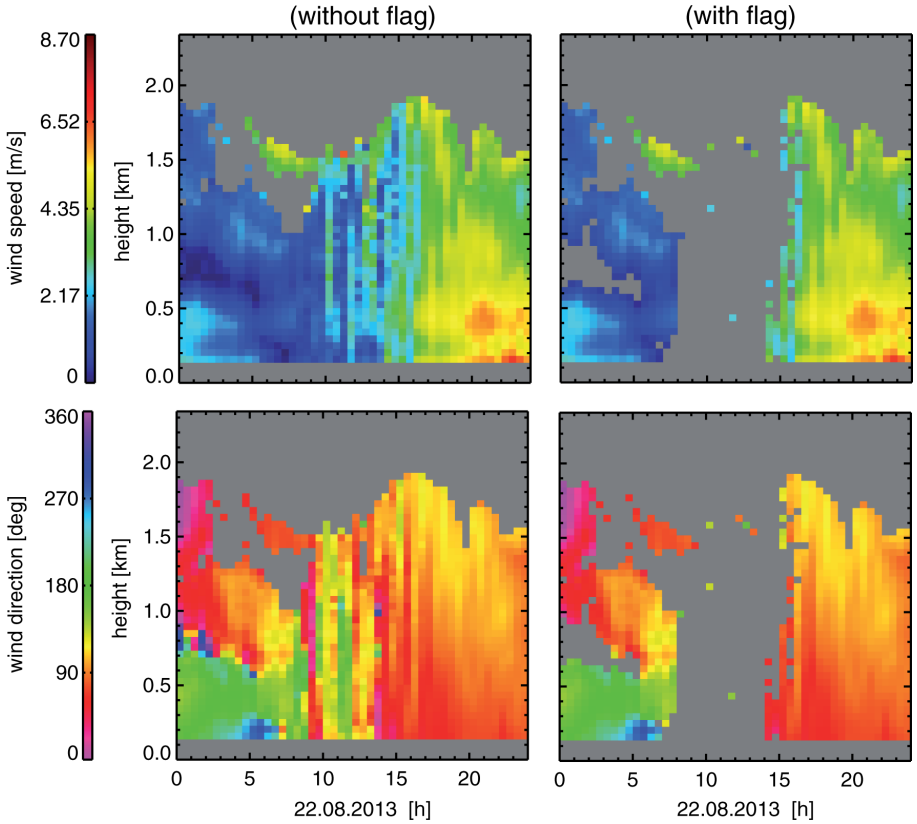

Figure 4. Left column: example for non-quality assured wind profile retrievals (top: wind speed, bottom: wind direction) from Doppler lidar measurements for a typical summer day (22 August 2013). Each profile represents a 30 min average. Right column: same wind retrievals as shown in the left column but where profiles with test parameters $R^2 < 0.95$ and CN > 10 have been discarded.

AMTD
7, 11439–11479, 2014

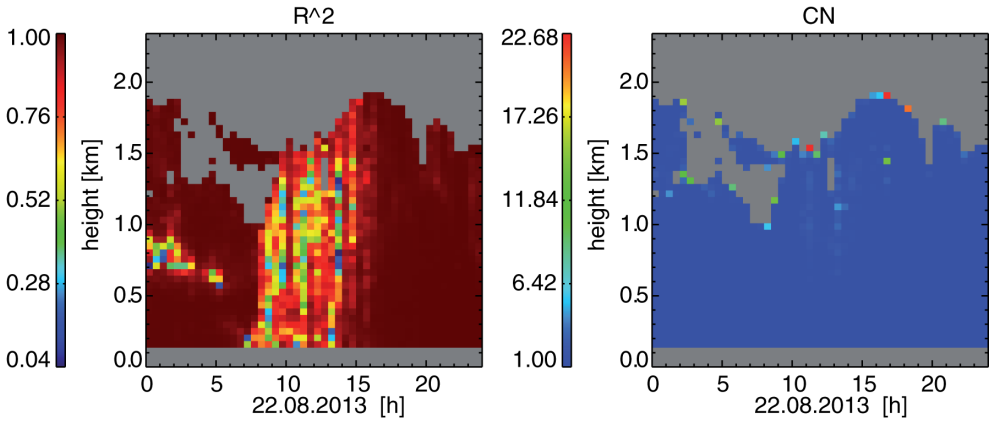

Figure 5. Calculated quality control parameters for the wind profiles shown in Fig. 4. R^2 is the coefficient of determination which provides a measure for the "goodness" of sine wave fit into the VAD Doppler velocity measurements. To ensure that the horizontal homogeneity assumption inherent to the wind vector retrieval is fulfilled, wind vector reconstructions with $R^2 < 0.95$ are classified as non reliable. Additionally, retrievals with $R^2 \geq 0.95$ are only valid for a condition number CN ≤ 10. The latter ensures a moderate degree of collinearity within the VAD scan Doppler velocity measurements.

AMTD
7, 11439–11479, 2014

A one year comparison of wind profile measurements

E. Päschke et al.

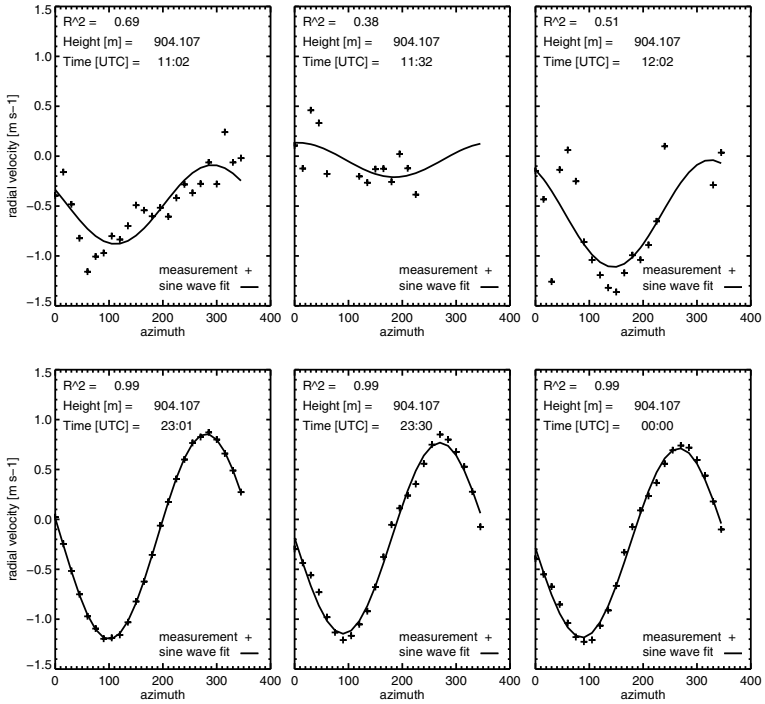

Figure 6. Examples for single sine wave fits into 30 min averaged VAD scans used to reconstruct the 30 min averaged wind profiles shown in Fig. 4 at 904 m height with the time stamps 11:02, 11:32 and 12:02 UTC (upper row) and the three time stamps 23:01, 23:30 and 00:00 UTC (lower row). The measurements in the upper line have been obtained during a well evolved CBL where horizontal homogeneous conditions are not met and which is also reflected in the low R^2 values. The measurements in the lower row have been obtained during stable atmospheric conditions at night. Here, the high values for R^2 indicate that the assumption of a horizontally homogeneous wind field is better fulfilled.

AMTD
7, 11439–11479, 2014

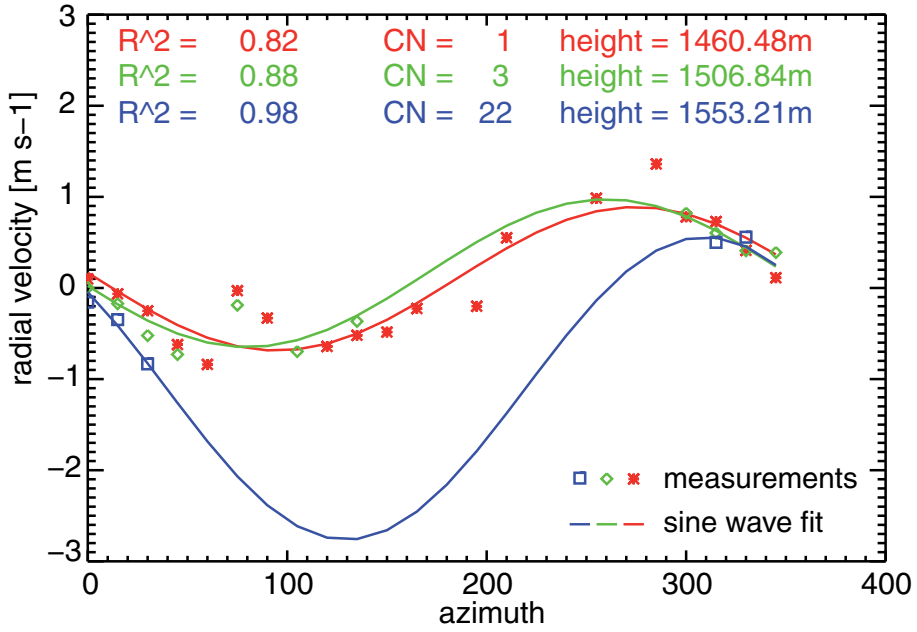

Figure 7. Examples for three sine wave fits used to reconstruct the 30 min averaged wind profiles shown in Fig. 4 at the three adjacent heights $h_1 = 1460.48$ m, $h_2 = 1506.84$ m and $h_3 = 1553.21$ m for the single time stamp 12:02 UTC. Additionally for each fit the quality control parameters R^2 and CN are also given. The sine wave fit at h_3 has a high R^2 but due to the large azimuthal gap size within the measurements the condition number CN is relatively high indicating a high degree of multicollinearity. The latter results in implausible magnitudes of the wind speed yielding unphysical vertical gradients in the wind speed field (see also the outstanding red pixel in the wind speed profile shown in Fig. 4 at the time stamp 12:02 UTC).

AMTD
7, 11439–11479, 2014

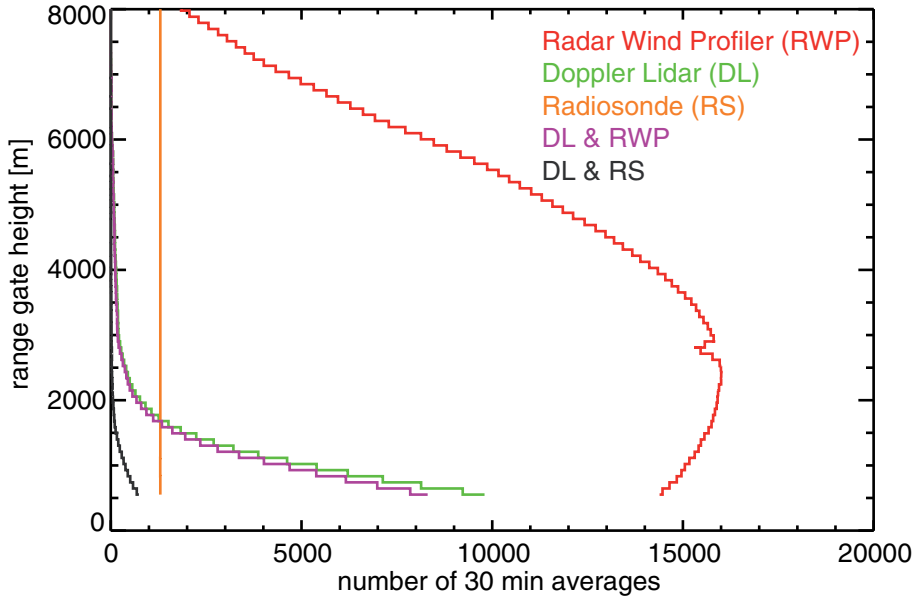

Figure 8. Overview of the data availability from one year measurements with Doppler Lidar (DL), Radar Wind Profiler (RWP) and Radiosonde (RS). Data availability refers to 30 min averaged profiles for wind speed and direction. The number of data used for the DLWR comparison is a subset of data indicated by DL & RWP where both systems provide valid data at the same time. The graph denoted with DL & RS reflects a subset of data where the DL and RS provide valid data at the same time and which have been used for the DLRS comparison.

AMTD
7, 11439–11479, 2014

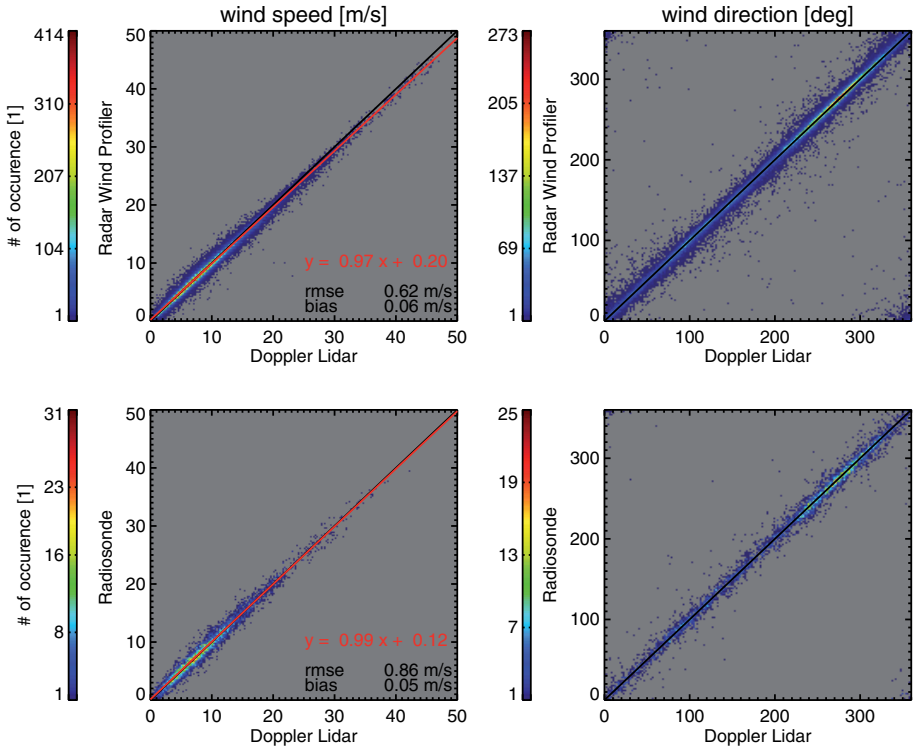

Figure 9. Top: scatter plots of one-year 30 min averaged horizontal wind speed and direction from Doppler Lidar and 482 MHz Radar Wind Profiler measurements (DLWR), bottom: scatter plots of one-year 30 min averaged horizontal wind speed and direction from Doppler lidar and Radiossonde (DLRS). Top and bottom: in principle all scatter plots include measurements from all heights.

AMTD
7, 11439–11479, 2014

A one year comparison of wind profile measurements

E. Päschke et al.

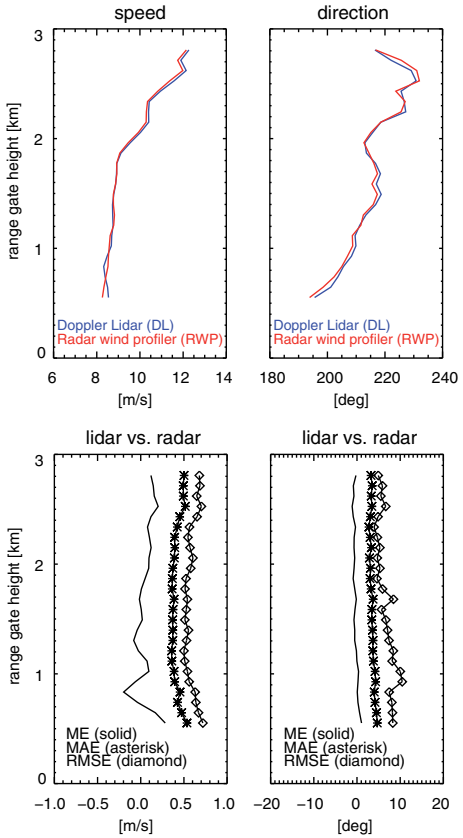

Figure 10. Statsitical results of the DLWR comparison. The upper two panels show the annual mean of wind speed and direction obtained from Doppler Lidar and Wind profiler measurements, respectively. Errorplots denoting the precision of the wind speeds in the annual profiles are not shown because of its very low magnitudes (see also the remarks in Sect. 3.1). The lower two panels show the respective verification scores ME (mean error), MAE (mean aboslute errors) and RMSE (root mean squared error).

AMTD
7, 11439–11479, 2014

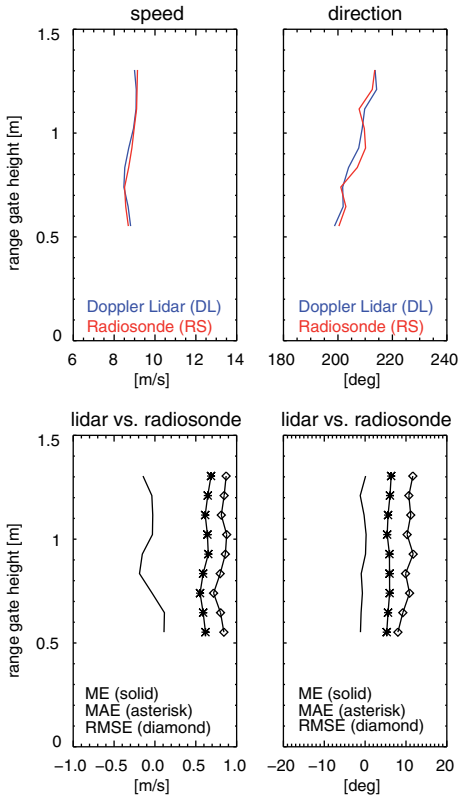

Figure 11. Same as in Fig. 10 but for the DLRS comparison.

AMTD
7, 11439–11479, 2014

A one year comparison of wind profile measurements

E. Päschke et al.

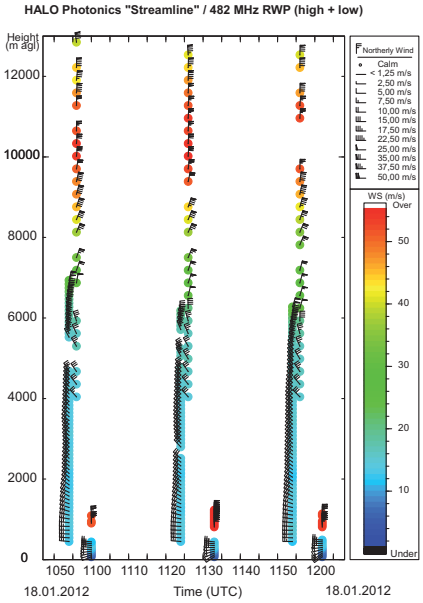

Figure 12. Comparison of wind profiles obtained from Doppler lidar measurements and wind profiler measurements on 8 January 2012 at the three different times (around 11:00, 11:30 and 12:00 UTC). For each time the wind profiler measurements are to the left and the Doppler lidar measurements are to the right. It can be observed that there are huge differences between the measurements around 1 km height. In particular, the winds measured with the Doppler lidar seem to be implausible due to the untypical strong wind speeds of about 60 m s^{-1}. If one takes a closer look to the (high mode) wind profiler measurements and taking the pulse repetition frequency (PRF = 15 kHz, see also Table 1) into account which defines the maximum measurement height Z_{max} = 10 km for the Doppler lidar used in this study these huge differences can be explained as follows. The wind profiler (high mode) measures winds of about 60 m s^{-1} in heights around 11 km. Also the Doppler lidar measures these winds but due to Z_{max} = 10 km the calcuation of the range is incorrect and the signals from the backscattering targets higher than 10 km are erroneously allocated to heights around 1 km.

AMTD
7, 11439–11479, 2014